NANO LETTERS

2007
Vol. 7, No. 5
1256−1263

Sensing Characteristics of NIR Localized Surface Plasmon Resonances in Gold Nanorings for Application as Ultrasensitive Biosensors

Elin M. Larsson,[†] Joan Alegret,[†] Mikael Käll,[†] and Duncan S. Sutherland*[,‡]

Department of Applied Physics, Chalmers University of Technology, S-41296 Göteborg, Sweden, and iNANO Center, University of Aarhus, Aarhus 8000, Denmark

Received January 21, 2007; Revised Manuscript Received March 16, 2007

ABSTRACT

The optical responses of 75–150 nm diameter gold nanorings to changes in local refractive index have been quantified by near-infrared extinction spectroscopy and compared to DDA calculations and an analytical approach. The "bulk" refractive index sensitivities of gold nanorings are substantially (>5 times) larger than those of nanodisks with similar diameters. Nanorings retain a significantly larger sensitivity than nanodisks at the same spectral position, demonstrating a clear shape dependence that may correlate to a systematic difference in the influence of the dielectric substrate. The nanoring bulk refractive index sensitivity scales linearly with plasmon peak position. The spectral sensitivity to thin films of alkanethiols gave a shift of ~5.2 nm/CH_2 unit while bulk sensitivities as high as 880 nm/RIU were observed, the highest such reported sensitivities. Both bulk and thin dielectric film sensitivities correlated well with theory. Real-time label-free monitoring of protein binding via molecular recognition was demonstrated.

The optical properties of noble metal nanoparticles have received significant research attention in recent years as a result of their potential applications as components in technologies as diverse as waveguides,[1] photonic circuits,[2] molecular rulers,[3] chemical/biological sensors,[4−7]and bioimaging agents.[8] The optical properties are dominated by the excitation of collective oscillations of the nanoparticles' conduction band electrons, called localized surface plasmon resonances (LSPRs), by the incoming electromagnetic waves. At the LSPR, the incoming light is absorbed or scattered by the nanoparticles, and concurrently, there is an electromagnetic field enhancement close to the particles. The energy of the LSPR depends on the particle size, shape, composition, interparticle spacing, and dielectric environment.[9] The later property opens a route to refractive index sensing where adsorbate-induced changes in the local dielectric environment is utilized for detection of molecular-binding events in the particle nanoenvironment.[10,11] Localized surface plasmons have been explored in a range of nanoparticle shapes such as disks,[12] triangles,[13] spheres,[14] cubes,[15] crescents,[16] and stars.[17] More complex structures, interpreted in terms of coupled plasmonic resonances, have also been widely studied including holes in thin metal films,[18] nanoshells,[19] nanorings,[20] and nanorice.[21] Major efforts have gone into studying the sensitivity of such structures to changes in the local refractive index as bulk or thin films,[14] with significantly increased bulk sensitivity values being reported for stars,[17] cubes,[15] and nanorice.[21] The potential for their use as ultrasensitive detectors of biomolecular recognition events comes from both the high refractive index sensitivity and short range of the associated optical fields.[14] The field profile has been studied theoretically[20,22] for a number of structures, with typical decays lengths (10−20 nm) being less than the size of the particles. While the small detection volumes open the potential to detect the binding of small numbers of unlabeled biomolecules, the associated short decay lengths complicate the detection of binding events by immunoassays, where antibody or antibody fragments immobilized on the nanoparticles move the molecular recognition event 5−10 nm from the surface where the sensitivity is reduced. An additional challenge when quantifying such interactions is to take into account the inhomogeneous field over the length scale of the adsorbing biomolecules. Theoretical calculations predict that the volume confined by nanorings[20] and nanoshells[22] has a relatively uniform enhanced electric field and may, therefore, be easier to apply in quantified biosensing applications. A number of different prototype LSPR refractive index sensors have been used to detect biological interactions including protein−ligand[7,10,11] DNA−DNA,[23]

* Corresponding author. E-mail: duncan@inano.dk. Telephone: +45 8942 5547. Fax: +45 8942 3690. Mobile: +45 2338 5789.
[†] Department of Applied Physics, Chalmers University of Technology.
[‡] iNANO Center, University of Aarhus.

10.1021/nl0701612 CCC: $37.00 © 2007 American Chemical Society
Published on Web 04/13/2007

carbohydrate−protein,[24,25] and lipid−protein[26] binding. The first nonmodel application of the LSPR nanosensor was demonstrated by Haes et al., who studied the interaction between molecules possibly involved in Alzheimer's disease.[7] Great efforts have also been made to extend the LSPR sensing scheme down to a single nanoparticle.[4,5,27−29] Increased refractive index sensitivity has been achieved by shifting LSPR resonances to longer wavelength, however, in many cases, this leads to significant increases in structure size and detection volume. One route to red-shifting resonances while retaining low interaction volumes has been to make use of plasmon hybridization in nanoshells,[19] nanorings,[20] nanorice,[21] and nanosandwiches.[30] Sun and Xia[31] showed that gold nanoshells exhibit larger LSPR peak shifts than solid gold nanospheres, with comparable diameters, provided that the particles experienced the same change of refractive index in their vicinity. Nanorings are a 2D analogue for nanoshells, where the empty core potentially is accessible for various sensing schemes at the nanometer scale.

Here we explore the LSPR resonance sensitivity of nanorings to bulk refractive index changes, demonstrating a linear relationship between sensitivity and spectral position for LSPR's situated in the near-infrared (NIR). A direct comparison of sensitivities of two structural features (nanorings and nanodisks) in the NIR is made with significantly higher sensitivities for nanorings at the same spectral positions. The sensitivity of nanoring LSPRs to thin dielectric films, with different thicknesses, is studied using self-assembled alkanethiol monolayers. As a proof of concept, we follow kinetically the adsorption of biotinylated albumin and subsequent molecular recognition of neutravidin in buffer.

Gold nanorings were prepared on soda lime or borofloat glass substrates using colloidal lithography, as described elsewhere.[20] The fabrication is schematically depicted in Figure 1a. In brief, polystyrene colloidal particles (50−140 nm diameter sulfate-modified latex, Interfacial Dynamics Corporation) were deposited, as sacrificial polymer masks, in a dispersed layer onto the glass substrates using electrostatic self-assembly. A 20 or 40 nm thick sacrificial gold film was, subsequently, thermally evaporated through the colloidal mask to act as local sputter source. A collimated argon ion beam was then used to etch away the gold film and, through secondary sputtering of material, create a gold shell around the undersides of the polystyrene particles. After removal of the remains of the polystyrene particles with UV-ozone treatment and subsequent water rinse, free-standing ringlike gold structures remained on the surface. Au disks were fabricated using hole−mask lithography.[32] Before use, samples used in bulk refractive index measurements and biosensing experiments were exposed to a solution of 80% ethylene glycol in deionized water (MilliQ), and samples used for chemosensing were exposed to ethanol for >12 h in order to saturate solvent-induced structural changes.[33] The morphology of each individual sample was characterized using atomic force microscopy (AFM) and scanning electron microscopy (SEM) to determine the height, outer diameter, and surface density of the nanorings. Ring-like gold structures with diameters between 75−150 nm were successfully fabricated. Parts b−e of Figure 1 show SEM images, from the top (b and d) and at 80° tilt (c and e), of nanorings with approximately 150 nm diameter on a silicon substrates. The electrostatic self-assembly of colloidal particle masks produces arrays of structures with a short-range order with a characteristic inter-ring spacing of 2−3 diameters (see ref 34 for details of the analysis approach). The approach of templating ring structures from sacrificial particles via secondary sputtering of local material produces highly circular individual rings with thin walls and smooth sides. The thinning of the walls toward the top of the ring structure can lead to roughening of the upper ridge. Such roughening does not appear to correlate to the optical properties but contributes to inhomogeneity, from structure to structure,

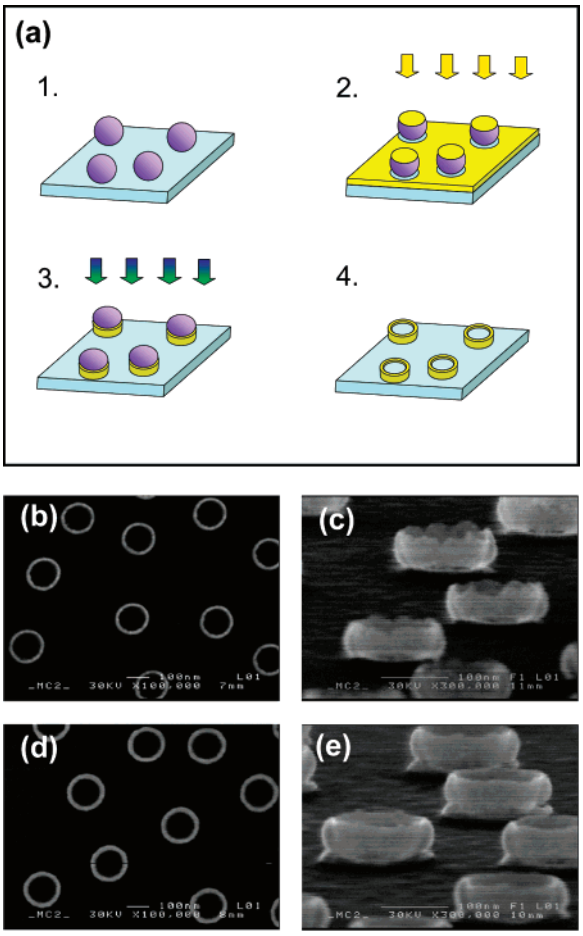

Figure 1. (A) Schematic depiction of the nanoring fabrication. (1) Polystyrene colloidal particles are deposited, by electrostatic self-assembly, onto the substrate in a dispersed layer. (2) A 20−40 nm thick gold film is evaporated onto the particle coated substrate at normal incidence. (3) Argon ion beam etching is used to remove the gold film. During the etching, secondary sputtering creates a gold shell around the base of the polystyrene particles. (4) The remainder of the polystyrene particles is removed by UV-ozone treatment, resulting in free-standing Au nanorings on the substrate. (B and C) SEM micrographs of 150 nm diameter gold nanorings made using a 20 nm thick sacrificial gold layer on a Si wafer substrate at normal incidence and 80° tilt respectively. (D and E) Gold nanorings (150 nm diameter) made using a 40 nm thick sacrificial gold layers at normal incidence and 80° tilt, respectively.

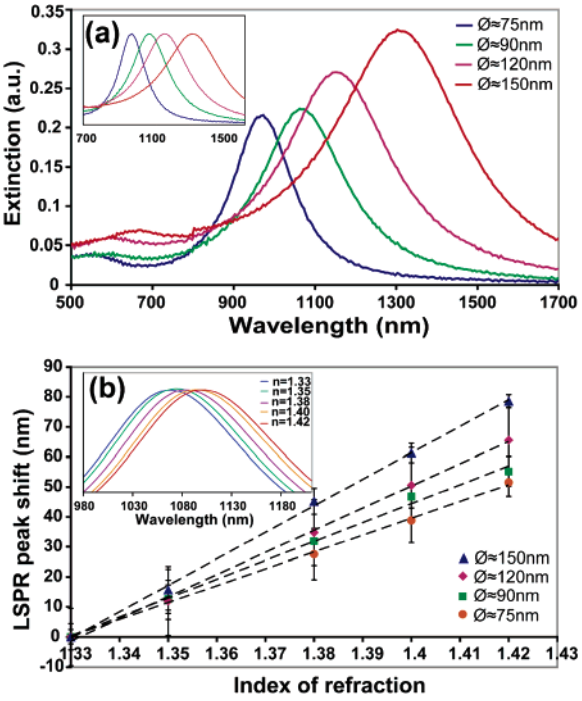

Figure 2. (A) Tuning of the LSPR peak wavelength by changing the diameter of the nanorings. The diameters given in the figure are average outer diameters. The inset shows the normalized extinction spectra. (B) LSPR peak shifts, relative to the peak positions in $n = 1.33$, when immersing the nanoring structures in different dielectric media. The inset shows the normalized spectra obtained when immersing 75 nm outer diameter rings in D_2O with varying concentrations of ethylene glycol. Error bars show standard deviations.

within the sample. By increasing the thickness of the Au film from 20 to 40 nm, the shape of the sidewalls can be changed and their thickness increased. This is shown in Figure 1, where the ring structures in parts b−c were made using a 20 nm thick sacrificial Au layer, while those in parts d−e were made using a 40 nm thick layer. The optical properties of systematically varied Au nanorings were investigated by optical extinction spectroscopy (measurements were made on a Cary 500 UV−vis−NIR spectrophotometer, using a sampling area of approximately 50 mm^2.)

Figure 2a shows the extinction spectra of nanorings with outer diameters approximately 75, 90, 120, and 150 nm made with a sacrificial film thickness of 20 nm. Nanorings exhibit a strong optical excitation in the NIR region of the spectrum. We have previously reported such excitations, which can be attributed to localized surface plasmon resonances confined within the ring geometry.[20] The nanoring LSPR's are red-shifted more than 400 nm from that of solid Au disks with similar diameters.[12] The wavelength of the nanoring LSPR is strongly dependent on the diameter of the nanorings, shifting to longer wavelengths as the diameter of the ring structures increases. Changing the diameter of the nanorings between 75−150 nm allowed tuning of the LSPR peak wavelength between approximately 1000−1300 nm. Increasing the thickness of the ring wall by evaporation of a thicker gold film caused the LSPR to shift to shorter wavelengths. This is in agreement with previously published theoretical and experimental results.[20]

We have investigated gold nanorings on glass substrates as potential label-free optical transduction elements in a nanoscale biosensor. Different refractive index environments were produced around nanoring samples in a liquid exchange cell, with a total volume of ∼110 μL, placed perpendicular to the incoming light beam. Bulk refractive index measurements were made by subsequently exchanging for liquids with varying refractive index and recording the extinction spectra. H_2O or D_2O with, respectively, 0, 20, 50, 70, and 90% ethylene glycol (EG) were used to obtain indexes of refraction ranging between 1.33 and 1.42, relevant for the detection of biological molecules in an aqueous environment. Liquids were exchanged so that the EG concentration was increased in steps from 0 to 90% and then decreased, in steps, back to 0%. In each series, a final measurement in a N_2 environment was made to ensure that the plasmon peak position had returned to its initial value. D_2O was used instead of H_2O to avoid complications associated with the absorption of electromagnetic radiation by H_2O molecules at wavelengths larger than ∼1400 nm. The H_2O resonances limit the spectral range at which useful biosensing can be performed in water using light transmission. However, the interference from H_2O light absorption may be avoided by using detection in total internal reflection mode.[35] Figure 2b shows the shift of the nanoring LSPR peak, measured by extinction spectroscopy, in bulk media with refractive index varied from 1.33 to 1.42 for nanorings with varying diameters. The spectral positions of the LPSR peaks were quantitatively determined from extinction spectra by measuring numerically the center of mass of the upper 10% portion of the peak after binning the data. Multiple measurements of refractive index sensitivity (minimum 3) were made for each sample and displayed as a standard deviation. An example of a bulk refractive index measurement going from 0 to 90% EG, for rings with 75 nm diameter, is shown in the inset of Figure 2b. A roughly linear shift of the LSPR peak to longer wavelength as the refractive index is increased in seen, which is in agreement with previously published data on, e.g., Au disks,[12] pits in Au film,[28] Au nanoshells,[31,36] and Ag triangles.[37] Experimentally, we obtained peak shifts per refractive index unit (RIU) ranging between 520−880 nm. For a given thickness of the Au sacrificial film, the nanoring sensitivity was observed to increase as the ring diameter increased. Increasing the Au film thickness caused the sensitivity to decrease. The recorded LSPR peak shifts with change in refractive index were significantly larger than those observed for Au disks[12] and pits,[18] made using a similar techniques, and Ag triangles.[37] Comparison of structures of similar size and material but of different shape yields a >5 times larger bulk refractive index sensitivity for nanorings over for example nanodisks.[11] The peak shifts for nanorings are of a similar order of magnitude to those observed for nanoshells[31,36] and nanorice,[21] which are hybridized systems similar to that of nanorings. The bulk sensitivity of 880 nm/RIU observed for 150 nm diameter rings formed with a 20 nm sacrificial gold layer is higher than that reported for nanoshells and nanorice and, to the best of our knowledge, is the highest reported for a nanoparticle system. The "figure

of merit" (FOM) was introduced by Sherry et al.[15] to directly compare the overall performance of single nanoparticles as chemical sensors. It is defined as the peak shift per refractive index unit divided by the full with at half-maximum, calculated in electron volts. The ensemble of structures reported here having bulk refractive index sensitivity ~880 nm/RIU has FOM ~2. However, single-particle measurements are needed to correct for inhomogeneous broadening and are likely to give significantly higher FOM values. Previously reported FOM values are 5.4[15] for single nanocubes and 10.7[17] for single nanostars.

For nanoring structures, we observe both a shift to longer wavelength of LSPR excitation and a larger sensitivity to bulk refractive index as the ring diameter is increased for a constant sacrificial gold layer thickness. A strong correlation between peak position and sensitivity to refractive index appears to exist. In Figure 3, LSPR sensitivity to changes in the bulk dielectric environment (i.e., peak shift per RIU), is plotted against the position of the LPSR peak for different nanorings. Ring samples were made using a 20 or 40 nm sacrificial gold layer. Those made with 20 nm gold layers had average outer diameters (and LPSR peak positions in $n = 1.33$): 75 nm (1058 ± 4 and 1122 ± 5nm), 90 nm (1255 ± 3 nm), 120 nm (1354 ± 10 nm), and 150 nm (1545 ± 1 nm). Rings made using a 40 nm sacrificial gold layer had average outer diameters (and LSPR peak positions in $n = 1.33$): 120 nm (1194 ± 4 nm) and 150 nm (1223 ± 3 nm). We observe a linear relationship between nanoring LSPR resonance position and LSPR sensitivity to bulk refractive index. This relationship holds true for all ring configurations tested. Aizpurua et al. used the dispersion relation for a thin slab to obtain an analytical model for the LSPR modes of a slablike ring. Assuming a Drude-like dielectric function for gold and a surrounding medium with a real dielectric function, the expression for the lowest-order symmetric (low-energy) mode reduces to

$$\lambda = \lambda_P \sqrt{n^2 \frac{1 + e^{-d/a}}{1 - e^{-d/a}} + \epsilon_0}$$

λ_P is the bulk plasmon wavelength, n the refractive index of the surrounding medium, ϵ_0 the dielectric function of gold, d the wall thickness, and a the radius of the ring. This model gives a similar linear relationship between LSPR peak position and sensitivity in the NIR region of the spectrum (solid line in Figure 3) as the experimental data although with a higher absolute sensitivity. The presence of a substrate that is not included in this analytical approach has been widely reported to influence the spectral position and measured refractive index sensitivity of LSPRs. A simple approach to take into account the substrate is to utilize an effective refractive index combining the substrate and surrounding dielectric properties and calculating the resultant spectral shifts for changes in surrounding refractive index. Assuming a substrate refractive index of 1.52 and that the shift induced by the substrate corresponds to around 17% of that induced when a nanoparticle is fully embedded in such a substrate, a good fit was obtained between the analytical approach and the experimental data (the dotted line in Figure 3). A relatively good fit could only be obtained with substrate influences in the range 15−19%.

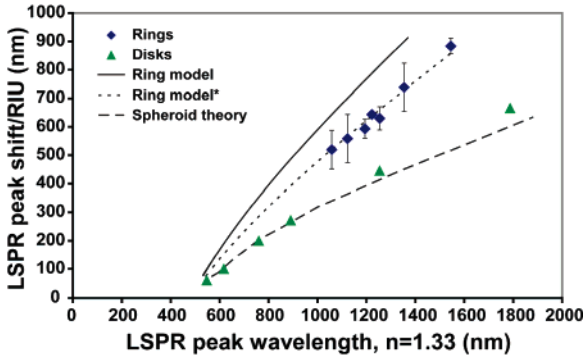

Figure 3. LSPR peak shift per refractive index unit as a function of the peak position for surrounding media $n = 1.33$. Experimental data for Au rings and disks is presented. Data for disks with peak wavelengths <800 nm is reproduced from Hanarp et al.[12] The solid and dotted lines were calculated using an analytical approach from Aizpurua et al.,[20] assuming 0% ("ring model") and 17% ("ring model*"), respectively, influence from the substrate to the total refractive index. The dashed line was calculated using spheroid theory and assuming a 50% influence from the substrate. Calculations were made for a change in surrounding refractive index from 1.33 to 1.42. Error bars show standard deviations. The error bars for disk samples were smaller than the figure symbols.

A structure-independent linear relationship between sensitivity and peak wavelength for gold structures below 130 nm in size and with resonance below ~800 nm was suggested by Miller and Lazarides.[38] The authors utilized numerical calculation approaches and did not include substrates. The suggested analytical approximation represents some type of upper limit to sensitivity. We investigated the structural dependence of the refractive index sensitivity of LSPRs with resonances in the near-infrared by comparing arrays of nanoring structures to arrays of nanodisks within the same spectral region. The spectral position of the disks was tuned into the NIR by tuning their aspect ratio. The bulk refractive index sensitivities of nanodisks of 20 or 25 nm height and made using 190−530 nm particles are plotted against spectral position (in $n = 1.33$) in Figure 3. Nanodisks with LSPRs in the visible region of the spectrum are reproduced from Hanarp et al. .[12] For Au structures supported at solid substrates with resonances in the NIR, we observed a significant structural dependence and a higher sensitivity for Au nanorings compared to nanodisks with a similar LSPR peak position.

The reported sensitivities for nanorice[21] fit with observed refractive index vs spectral position relationship seen in Figure 3. However, we report a higher absolute sensitivity for nanorings at longer wavelengths: ~880 nm/refractive index unit.

Electrostatic ellipsoid theory was used to estimate the bulk refractive index sensitivities for nanodisks by approximating the disks with an oblate spheroid. The spheroid was treated as an induced dipole for which the dipolar polarizability was calculated as a function of spheroid geometry and bulk dielectric response functions of the metallic particle and the

surrounding dielectric medium. For larger spheroids, finite wavelength effects were taken into account by adding a radiation damping and a dynamic depolarization term to the polarizability function.[32] By calculating LSPR resonance positions for specific structural aspect ratios in different refractive index media, the bulk refractive index sensitivity was obtained. In the same way as was done in the analytical model for rings, we took into account the substrate by utilizing effective refractive indices, calculated by including a contribution from both the substrate and the surrounding medium and correlating changes in spectral position to changes in surrounding media refractive index. We obtained a good correlation between the theoretically determined and experimental bulk sensitivities vs spectral position for including a substrate effect of 50% (dashed line in Figure 3).

Within the same spectral range, we observe a marked difference in the apparent influence of the substrate on nanorings (∼17%) and nanodisks (∼50%). That a good fit between theory and experiment is obtained for all the rings studied for a single effective substrate condition implies that there is a systematic difference in the influence of the substrate related to the shape of the nanoparticle. Dielectric material placed close to the metal surface of a nanoparticle has a strong influence on the spectral position of the LSPR.[14] A crude approach to estimating the relative effect of a substrate on localized surface plasmons supported in different nanoparticles is to utilize a parameter reflecting percentage of the nanoparticle in the vicinity of the substrate. We estimated the percentage of the surface area of the different ring and disk nanoparticles in direct contact with the substrate, utilizing an idealized geometry with vertical side walls and constant wall thickness, obtaining 19−29% for rings and 41−46% for disks in the same spectral region, depending on the specific geometry of each particle type. The percentage contact areas fit qualitatively with the substrate effects obtained from fitting. In reality, the ring geometries are nonideal, being narrower at the top and bottom, suggesting that the substrate contact percentages for rings are overestimated. Interestingly, utilizing a 50% substrate effect for the rings calculation yields a reasonably good fit to the experimental disk data, and likewise utilizing a 17% substrate for a simple ellipsoid theory yields a relatively good fit for the experimental ring data. These results suggest that a significant part of the structure dependent difference in refractive index sensitivity observed between nanorings and nanodisks in the NIR (and by implication many other structures) may result from systematic differences in the influence of the substrate. Design of surface-bound nanostructures with minimized LSPR near-field overlap with the substrates may provide a route to enhanced sensitivity nanoscale optical biosensors.

We demonstrate that localized surface plasmon resonances in nanorings are highly sensitive to changes in the surrounding bulk refractive index with potential for use as sensors. The application of such systems for the detection of molecular recognition or binding events typically involves the change of refractive index of thin films close to the metal surface rather than bulk changes. The sensing characteristics under such conditions are expected to be influenced by both the bulk sensitivity and the profile and homogeneity of the decay of the optical field away from the particle surface. We performed chemosensing experiments with alkanethiol self-assembled monolayers of defined thickness to investigate the sensitivity of the LSPR's to thin dielectric layers.

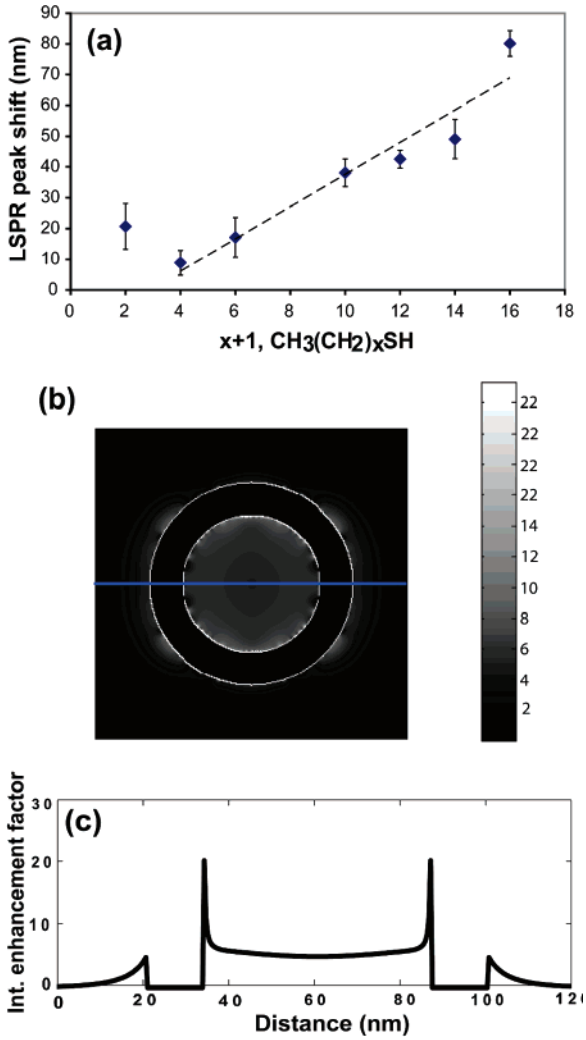

Figure 4. (A) LSPR peak shifts measured after adsorption of alkanethiols onto 75 nm outer diameter Au rings. Extrapolating a trend line fitted to the data points obtained for 4−16 carbon alkanethiols, gives the intercept 15 nm. Error bars show standard deviations. (B) Intensity enhancement factor calculated at mid-height of a ring structure surrounded by $n = 1.00$ media. (C) Intensity enhancement factor along the blue line in figure b.

Figure 4a shows LSPR peak shifts caused by the adsorption of varying length alkanethiols to nanorings with 75 nm outer diameter. By varying the length of the thiols, high refractive index layers of varying thickness can be formed on the nanorings. Measurements were performed with straight chain alkanethiols having 2, 4, 6, 10, 12, 14, and 16 carbons, respectively. The samples were rinsed in water, dried with N_2 gas, and extinction spectra recorded before incubating in ∼5 μg/mL thiol in ethanol for >24 h. Physisorbed thiol was removed by immersing the samples in ethanol over night. After rinsing in water, the samples were dried with N_2 gas and extinction spectra recorded.

Ethanethiol gave rise to larger peak shifts than butanethiol, most likely because the ethanethiol molecules are too short to form a well organized layer under the conditions used here. In agreement with previous publications,[28,29,33] we find that the LSPR peak red-shifts linearly with increasing number of carbon atoms, $x + 1$, in the alkanethiol molecule for $x \in [3-15]$. For gold nanorings, the peak shift per carbon atom was found to be about ~5.2 nm. This can be compared to 0.7 nm found for hole arrays in an Au film[28] and 4.4 nm found for single Ag nanoprisms.[29] The thin film sensitivity observed here is the highest reported for a nanoparticle system. The linear regime extrapolates to a negative peak shift of ~15 nm for the thiol group (i.e., without any carbons). This shift is of the same magnitude (although slightly larger) than has previously been observed for Au[28] and Ag[5,33] nanostructures.

Combining the information obtained from the bulk refractive index measurements and the thiol adsorption experiments allows the estimation of the spatial extent, i.e., the decay length δ of the induced field. In general, this is done by calculating an average refractive index for the adsorbed layer and the surrounding medium, using the intensity of light at each point as the weighing factor, which then determines the plasmon wavelength through the appropriate resonance condition.[39] This method has previously been used to estimate the decay length in holes in an Au film.[28] Assuming that the field decays exponentially away from the surface, that the refractive index of the thiol layer is 1.5, and that the thickness increase per CH_2 group is 0.12 nm,[40] gives the decay length $\delta = 12$ nm. This value is similar to that obtained for nanoholes in Au film[28] and much smaller than that expected for LSPRs at disks in the same wavelength region.[41] These results indicate that Au nanorings are highly sensitive to refractive index changes in their direct vicinity.

We have investigated the optical field profile around idealized gold nanoring structures by DDA calculations.[42,43] The calculated field plot around a 75 nm outer diameter ring (10 nm wall thickness) with vertical walls is shown in Figure 4b and c. A relatively uniform intensity enhancement factor $(E/E_0)^2 \approx 5$ is seen inside the ring cavity, well in line with previously reported calculations based on the boundary charge method (BCM).[20] This result is also in qualitative agreement with previously published DDA results on nanoshells.[22] The high field enhancement over a significant volume suggests that the inside of nanorings may provide suitable sites for detection of molecular-binding events for biosensor applications. However, in nanorings, unlike in conventional nanoshells, the region inside the particle is generally accessible to biomolecules in the surrounding media, making nanorings advantageous for use in such applications. The field outside of the rings decays rapidly away from the outer ring wall. To estimate the decay length of the electromagnetic field, we assumed an exponential decay with a characteristic decay length. An exponential field decay is correct for a planar metal film, while for the induced field away from a metal nanoparticle, it is a useful approximation.[28] Fitting an exponential function to the field picture obtained by taking a 2D slice, through the center of the ring and along the polarization direction of the incident light, gives the decay length of ~8 nm from the outer wall of the ring. The field inside the ring is observed to decay with an estimated decay length of a few nanometers, which is likely to be a result of artifacts from the DDA approach, which here utilizes a discrete mesh size of 2 nm, making estimation of the field decay very close to the surface difficult. At longer distances (>5 nm) from the surface, a slower decay is seen with a decay length of the order of 24 nm. The agreement between the experimentally determined decay length for the corresponding nanorings of ~12 nm, which is the average decay length for the whole structure, and that determined from DDA-calculated field plots (8 nm outer wall and 24 nm inner wall) is surprisingly good given that DDA calculations are not expected to give field information on the length scale of the thiols (<2 nm).

Higher absolute bulk sensitivity for nanoparticle structures can be obtained by producing appropriate shapes of structures with resonances in the NIR. For nanodisks and other simple plasmonic structures, this typically leads a significant increase of size of structures with concomitant increase in the detection volume. Larger detection volumes require larger numbers of molecules to fill them and the sensitivity per molecule adsorbed may actually decrease as larger structures with longer wavelength and more "bulk" sensitive resonances are utilized. Nanorings in common to nanoshells,[19] nanorice,[21] and nanosandwiches[30] can produce resonances in the NIR for still relatively small structures. On the other hand, short optical decay lengths with associated short sensitivity ranges can complicate the detection of macromolecules, where both the capture molecule and analyte often have significant physical size. The detection event may be occurring 5−10 nm from the surface (significantly further for immunoassays if whole antibodies rather than antibody fragments are used). The elevated field within the nanorings (see Figure 4b) may well provide a well defined and small region suited to the detection of macromolecules.

Ordered arrays of diamond-shaped nanorings have recently been reported formed via nanoimprint lithography.[44] Although no quantification of refractive index sensitivity was carried out, the LSPR shifts for the binding of streptavidin to surface-bound biotin was monitored after drying and compared to ring arrays in air. In common to other LPSR-based biosensing measurements made in air,[11,28] relatively large shifts for organic overlayers are seen resulting from the relatively higher refractive index contrast of air to organic material (1−1.42). Although it is difficult to rule out the contribution of long-range ordered diffractive coupling between the diamond ring structures, these experiments indicate that nanorings have significant potential for detecting biomolecular-binding events.

In a proof of principle experiment that nanorings can be used in real-time biosensing experiments, model experiments were carried out in buffer to kinetically monitor protein adsorption and molecular recognition events, see Figure 5a. Samples with ring structures of 75 nm diameter were used (LSPR in buffer 1119 ± 36 nm). Extinction spectra were recorded every 30 s. The protein-binding steps are schemati-

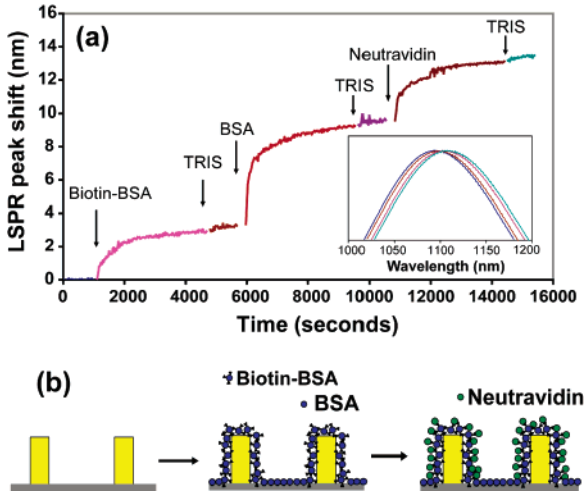

Figure 5. (A) LSPR peak shift as a function of time for adsorption of biotin-BSA and subsequently BSA onto 75 nm outer diameter rings on a soda lime glass substrate. The peak shift caused by the binding of neutravidin to biotinylated BSA is also shown. BSA was used to block the binding of neutravidin to the glass substrate. The inset shows the LSPR peak in buffer before the experiment and after the adsorption/binding of each protein. The LSPR in buffer was 1096 nm. (B) Schematic showing the binding of biotin-BSA, BSA, and neutravidin to Au nanorings immobilized on a glass substrate.

cally depicted in Figure 5b. First, biotinylated bovine serum albumin (biotin-BSA, Sigma-Aldrich) was adsorbed onto the gold structures. Biotin-BSA has previously been shown to bind preferentially to gold over SiO_2 during the conditions used here (10 μg/mL in TRIS buffer, pH 8.0).[45] The glass surface was subsequently blocked for protein binding by adsorbing BSA (5 mg/mL, Sigma-Aldrich) before adding neutravidin solution (10 μg/mL, Nordic Biolab). Unbound proteins were removed by rinsing with buffer. Biotin-BSA binding resulted in peak shifts of 4.9 $\pm$ 1.4 nm, while BSA binding gave slightly larger peak shifts, 6.4 $\pm$ 0.2 nm. The larger peak shifts observed for BSA binding to the glass substrate are not surprising because, even though the field decays rapidly away from the nanoring, DDA modeling predicts a relatively large area with enhanced field inside the ring cavity. Neutravidin binding gave rise to 3.7 $\pm$ 0.3 nm peak shifts. It has been shown that, on a flat Au surface, the mass uptake of neutravidin on biotin-BSA is about twice as high as the mass uptake of biotin-BSA on Au.[28] In our experiments, we observed a slightly smaller peak shift for the neutravidin binding than the biotin-BSA binding, supporting the data indicating a rapid decay of the electromagnetic field away from the particle surface. Control experiments were made where the biotin-BSA step was omitted. Very little neutravidin binding was observed in these experiments, showing that BSA is reasonably effective in blocking the surface. The BSA binding to all parts of the surface in the control experiments gave rise to 13.4 $\pm$ 1.4 nm peak shifts.

The LSPR shift observed for the binding of monolayers of biotin-BSA to gold nanorings ($\sim$5 nm) results from $\sim$360 proteins binding to the surface of each ring (calculated from biotin-BSA binding on flat gold surfaces under identical conditions[45]). While the experiments performed here investigated mm^2 areas of rings, the bulk and thin film sensitivity of nanorings suggest that single-particle measurements might have the potential to detect the binding of small ($<$10) numbers of molecules label free. While the observed optical extinction maxima have relatively broad peaks in the extinction spectra obtained from ensemble measurements, the width of the peak is partially a result of inhomogeneous broadening. It is expected that the spectra from individual nanoring particles would have considerably narrower peaks.[29]

LSPRs in gold nanorings exhibit extinction maxima in the NIR. The resonances are substantially red-shifted compared to similarly sized disks, and this red-shift is accompanied by a substantial increase in bulk refractive index sensitivity ($>$5 times). Larger-diameter rings show increasing red-shifts with a linear relationship between spectral position and bulk refractive index sensitivity being observed (with values up to 880 nm/RIU being measured). Disks in the same spectral region show significantly lower sensitivities. Simple analytical approaches gave qualitatively good fits for both nanorings and nanodisks. The effect of the substrate appeared to be systematically lower for nanorings compared to nanodisks, which may contribute to the enhanced bulk sensitivity of nanorings over nanodisks in the same spectral region. Chemosensing experiments with alkanethiol self-assembled monolayers showed a sensitivity of 5.2 nm/CH_2 group with an average sensitivity decay length of 12 nm, which correlated well with DDA predictions of 8 nm decay length for the outer wall and 24 nm for the inner wall of the ring structures. Simple kinetic biosensing experiments showed substantial spectral shifts for protein layers adsorbing from buffer ($>$13 nm for a BSA monolayer) and demonstrated the real-time detection of molecular-binding events, suggesting nanorings as potential ultrasensitive refractive index biosensor platforms.

References

(1) Hutter, E.; Fendler, J. H. *Adv. Mater.* **2004**, *16*, 1685−1706.
(2) Ozbay, E. *Science* **2006**, *311*, 189−193.
(3) Reinhard, B. M.; Siu, M.; Agarwal, H.; Alivisatos, A. P.; Liphardt, J. *Nano Lett.* **2005**, *5*, 2246−2252.
(4) Mock, J. J.; Smith, D. R.; Schultz, S. *Nano Lett.* **2003**, *3*, 485−491.
(5) McFarland, A. D.; Van Duyne, R. P. *Nano Lett.* **2003**, *3*, 1057−1062.
(6) Elghanian, R.; Storhoff, J. J.; Mucic, R. C.; Letsinger, R. L.; Mirkin, C. A. *Science* **1997**, *277*, 1078−1081.
(7) Haes, A. J.; Hall, W. P.; Chang, L.; Klein, W. L.; Van Duyne, R. P. *Nano Lett.* **2004**, *4*, 1029−1034.
(8) El-Sayed, I. H.; Huang, X. H.; El-Sayed, M. A. *Nano Lett.* **2005**, *5*, 829−834.
(9) Kreibig, U.; Vollmer, M., *Optical Properties of Metal Clusters*; Springer-Verlag: Berlin, Germany, 1995; Vol. 25.
(10) Nath, N.; Chilkoti, A. *Anal. Chem.* **2002**, *74*, 504−509.
(11) Haes, A. J.; Van Duyne, R. P. *J. Am. Chem. Soc.* **2002**, *124*, 10596−10604.
(12) Hanarp, P.; Kall, M.; Sutherland, D. S. *J. Phys. Chem. B* **2003**, *107*, 5768−5772.
(13) Jensen, T. R.; Schatz, G. C.; Van Duyne, R. P. *J. Phys. Chem. B* **1999**, *103*, 2394−2401.
(14) Okamoto, T.; Yamaguchi, I.; Kobayashi, T. *Opt. Lett.* **2000**, *25*, 372−374.
(15) Sherry, L. J.; Chang, S. H.; Schatz, G. C.; Van Duyne, R. P.; Wiley, B. J.; Xia, Y. N. *Nano Lett.* **2005**, *5*, 2034−2038.
(16) Shumaker-Parry, J. S.; Rochholz, H.; Kreiter, M. *Adv. Mater.* **2005**, *17* (17), 2131−2134.

(17) Nehl, C. L.; Liao, H. W.; Hafner, J. H. *Nano Lett.* **2006**, *6*, 683−688.
(18) Prikulis, J.; Hanarp, P.; Olofsson, L.; Sutherland, D.; Kall, M. *Nano Lett.* **2004**, *4*, 1003−1007.
(19) Averitt, R. D.; Sarkar, D.; Halas, N. J. *Phys. Rev. Lett.* **1997**, *78*, 4217−4220.
(20) Aizpurua, J.; Hanarp, P.; Sutherland, D. S.; Kall, M.; Bryant, G. W.; de Abajo, F. J. G. *Phys. Rev. Lett.* **2003**, *90*, 057401.
(21) Wang, H.; Brandl, D. W.; Le, F.; Nordlander, P.; Halas, N. J. *Nano Lett.* **2006**, *6*, 827−832.
(22) Schelm, S.; Smith, G. B. *J. Phys. Chem. B* **2005**, *109*, 1689−1694.
(23) Olofsson, L.; Rindzevicius, T.; Pfeiffer, I.; Kall, M.; Hook, F. *Langmuir* **2003**, *19*, 10414−10419.
(24) Yonzon, C. R.; Jeoungf, E.; Zou, S. L.; Schatz, G. C.; Mrksich, M.; Van Duyne, R. P. *J. Am. Chem. Soc.* **2004**, *126*, 12669−12676.
(25) Morokoshi, S.; Ohhori, K.; Mizukami, K.; Kitano, H. *Langmuir* **2004**, *20*, 8897−8902.
(26) Dahlin, A.; Zach, M.; Rindzevicius, T.; Kall, M.; Sutherland, D. S.; Hook, F. *J. Am. Chem. Soc.* **2005**, *127*, 5043−5048.
(27) Raschke, G.; Kowarik, S.; Franzl, T.; Sonnichsen, C.; Klar, T. A.; Feldmann, J.; Nichtl, A.; Kurzinger, K. *Nano Lett.* **2003**, *3*, 935−938.
(28) Rindzevicius, T.; Alaverdyan, Y.; Dahlin, A.; Hook, F.; Sutherland, D. S.; Kall, M. *Nano Lett.* **2005**, *5*, 2335−2339.
(29) Sherry, L. J.; Jin, R. C.; Mirkin, C. A.; Schatz, G. C.; Van Duyne, R. P. *Nano Lett.* **2006**, *6*, 2060−2065.
(30) Dmitriev, A.; Pakizeh, T.; Kall, M.; Sutherland, D. S. *Small* **2007**, *3*, 294−299.
(31) Sun, Y. G.; Xia, Y. N. *Anal. Chem.* **2002**, *74*, 5297−5305.
(32) Langhammer, C.; Yuan, Z.; Zoric, I.; Kasemo, B. *Nano Lett.* **2006**, *6*, 833−838.
(33) Malinsky, M. D.; Kelly, K. L.; Schatz, G. C.; Van Duyne, R. P. *J. Am. Chem. Soc.* **2001**, *123*, 1471−1482.
(34) Hanarp, P.; Sutherland, D.; Gold, J.; Kasemo, B. *Nanostruct. Mater.* **1999**, *12*, 429−432.
(35) Sonnichsen, C.; Geier, S.; Hecker, N. E.; von Plessen, G.; Feldmann, J.; Ditlbacher, H.; Lamprecht, B.; Krenn, J. R.; Aussenegg, F. R.; Chan, V. Z. H.; Spatz, J. P.; Moller, M. *Appl. Phys. Lett.* **2000**, *77*, 2949−2951.
(36) Tam, F.; Moran, C.; Halas, N. *J. Phys. Chem. B* **2004**, *108*, 17290−17294.
(37) Jensen, T. R.; Duval, M. L.; Kelly, K. L.; Lazarides, A. A.; Schatz, G. C.; Van Duyne, R. P. *J. Phys. Chem. B* **1999**, *103*, 9846−9853.
(38) Miller, M. M.; Lazarides, A. A. *J. Phys. Chem. B* **2005**, *109*, 21556−21565.
(39) Jung, L. S.; Campbell, C. T.; Chinowsky, T. M.; Mar, M. N.; Yee, S. S. *Langmuir* **1998**, *14*, 5636−5648.
(40) Shi, J.; Hong, B.; Parikh, A. N.; Collins, R. W.; Allara, D. L. *Chem. Phys. Letters* **1995**, *246*, 90−94.
(41) Gunnarsson, L.; Rindzevicius, T.; Prikulis, J.; Kasemo, B.; Kall, M.; Zou, S. L.; Schatz, G. C. *J. Phys. Chem. B* **2005**, *109*, 1079−1087.
(42) Draine, B. T. *Astrophys. J.* **1988**, *333*, 848−872.
(43) Purcell, E. M.; Pennypac, Cr. *Astrophys. J.* **1973**, *186*, 705−714.
(44) Kim, S.; Jung, J. M.; Choi, D. G.; Jung, H. T.; Yang, S. M. *Langmuir* **2006**, *22*, 7109−7112.
(45) Svedhem, S.; Pfeiffer, I.; Larsson, C.; Wingren, C.; Borrebaeck, C.; Hook, F. *Chembiochem* **2003**, *4*, 339−343.

NL0701612